When do contrails cool the atmosphere?

Judith Rosenow and Hartmut Fricke

Institute of Logistics and Aviation
Technische Universität Dresden
Dresden, Germany

***Abstract*—One of the main causes of aviation-induced climate change is the formation of contrails. To quantify how much of an impact contrails in general have on global warming, lots of thorough research has been done. Individual contrails might even decide on a cooling and a warming effect. This effect can be in the same order of magnitude as the climate impact of aviation-emitted carbon dioxides and nitrogen oxides. Therefore, three-dimensional optical and meteorological investigations of individual contrails have been performed. This paper focuses on conditions of contrails with a cooling effect on global warming. We found, that a flat sun position during sunrise and sunset increases the possibility of a solar cooling effect dominating the terrestrial heating effect. Individual contrails additionally benefit from flight paths between East and West due to an increased travelling distance of photons through the contrail. On a small scale, the outcomes can be applied to arbitrary trajectory optimization tools with a focus on environmental optimization. On a large scale, the results can be used in environmentally optimized Air Traffic Flow Management.**

***Keywords*—Contrails, Aviation, Environmental Impact, Radiative Forcing**

I. Introduction

When water vapour emissions and ambient humidity condense around exhausted soot particles and atmospheric condensation nuclei in a cold ambient atmosphere, a type of human-induced cloud known as a condensation trail (contrail) is formed, satisfying the Schmidt-Appleman-criterion [1, 2]. According to the World Meteorological Organization [3], these man-made ice clouds transform into long-lasting cirrus clouds known as "Cirrus homogenitus" in an ice-supersaturated environment. Contrails function as a barrier to the energy budget of the Earth's atmosphere [4–6]. They scatter incoming shortwave solar radiation back to the sky (resulting in a cooling effect) and absorb and emit outgoing longwave terrestrial radiation back to the Earth's surface (yielding a warming effect in the lower layer of the atmosphere) [5, 7–9].

The dominant effect can be described by the radiative forcing RF, as an imbalance in the net energy exchange between Earth and the atmosphere in the tropopause (taking into account the instantaneous reaction of the stratosphere) [5]. The precise amount of contrails' RF is yet unknown and is dependent on flight efficiency, the environment, and the time of day. Recent combinations of several modelling techniques to simulate the effects of contrails on global warming result in a warming net effect for 2010 of $RF_{\mathrm{Contrail}} = 0.05$ W m-2 with accuracy between -0.02 and $+0.15$ W m$^{-}2$ [5]. Single studies provide a precise assessment of the environmental consequences of contrails, including their cooling-related negative net effects (e.g., $RF_{\mathrm{Contrail}} = -0.007$ to $+0.02$ W m$^{-}2$ for 2005 [8]. Using global climate models and historical air traffic data, accurate projections of the global contrail radiative forcing for the year 2000 of $RF_{\mathrm{Contrail}} \approx 0.03$ (-0.01 to $+0.08$) W m$^{-}2$ [8] have been improved for 2010 to $RF_{\mathrm{Contrail}} \approx 0.02$ W m$^{-}2$ (-0.01 to $+0.03$) W m$^{-}2$ [5] considering an increased air traffic volume by 22 % between 2005 and 2010. In a global climate model for the year 2002, Burkhardt and Kärcher [9] estimated that the contribution of contrails and contrail cirrus to aviation's radiative forcing was $RF_{\mathrm{Contrail}} = 0.03$ W m$^{-}2$.

However, the uncertainties in determining the net radiative forcing of contrails arise, among other things, from the fact that contrails can cool the troposphere under certain conditions. This happens as soon as the solar cooling effect dominates the warming terrestrial effect. Therefore, the radiative effect of single contrails has to be investigated. This paper investigates in formation conditions of cooling contrails by applying a three-dimensional optical model to single contrails.

The question arises, when do contrails cool the atmosphere? Can we use this knowledge to minimize the climate impact of aviation?

Even hydrogen-powered aircraft can induce contrails by emitting water and fulfilling the Schmidt-Appleman-criterion [10].

A. State of the Art

There are two main approaches for investigating the effect of contrails on global warming. First, local investigations in single contrails as done by Gounou et al. [11] and Forster et al. [12], examined the radiative effect of single contrails, concentrating on the significance of large solar zenith angles at sunset and sunrise by applying a Monte Carlo code for photon transport in a coarse spatial grid and by ignoring the effect of flight performance on the optical characteristics of the contrail. At least, phenomena like multiple scattering are into account. Schumann et al. [13, 14] developed the Contrail Cirrus prediction tool CoCiP, an empiric and parametric radiative forcing model calculating the radiative extinction of single contrails with a low dependency on solar zenith angle and particle radius. The time of day is only reflected in the weak dependence on the solar zenith angle. Optical properties are only parameterized for radiant fluxes which have already been integrated over a hemisphere. This means that no angular dependence due to the time of day or the spatial orientation of the contrail can be taken into account.

Assuming a constant optical depth, Avila and Sherry [15] applied a model created by Schumann et al. [14] to assess the radiative forcing of individual contrails. Here, the optical depth, width, and particle diameter of contrails are generally parameterized. According to Schumann, an effective particle radius is roughly calculated for each contrail class, and each effective radius relates to particular optical characteristics. The fact that the solar zenith angle was taken into account in the study by Avila and Sherry is a significant advantage.

Rosenow [16, 17] has developed thorough investigations with a granular spatial resolution and considering all possible solar zenith angles in order to allow investigations of all day times.

Second, climate models are used for global investigations by treating contrails as an endless homogeneous artificial cloud layer. For example, the Adjusted Forcing AF as an imbalance of the Earth-atmosphere energy system has been calculated using satellite data, taking into account a completed transition of contrails into cirrus after stratospheric temperatures and adjusted to regain a radiative equilibrium in the stratosphere (assuming zero further radiative heating rates) [18, 19]. Here, it is possible to distinguish between regions with low and high demand for air traffic as well as the daily cycle of contrails and cirrus [19]. $AF_{\mathrm{Contrail}} = 0.045$ to 0.075 $\mathrm{W\,m^{-2}}$ has been quantified for contrails and contrail-induced cirrus using satellite data from 2006.

A contrail and contrail-induced cirrus AF_{Contrail} for the year 2010 of $AF_{\mathrm{Contrail}} = 0.05$ $(0.02$ to $0.15)$ $\mathrm{W\,m^{-2}}$ is widely accepted [5] for the year 2010 based on a combination of modelled and satellite data-based estimates with tolerances in spreading rate, contrails optical depth, ice-particle shape, and radiative transfer, as well as accounting for the ongoing increase in air traffic [20].

Assuming $RF_{\mathrm{Contrail}} = 0.049$ $\mathrm{W\,m^{-2}}$ in 2006 and taking into account a change in cruising altitudes, an increase in air traffic distance until 2050 by a factor of 4 compared to 2006, an increase in alternative fuels (with reduced soot emission), and anticipated changes in propulsion efficiency in 2050, Bock and Burkhardt [21] predicted a global future contrail radiative forcing of $RF_{\mathrm{Contrail}} = 0.159$ $\mathrm{W\,m^{-2}}$. The global distribution of the anticipated air traffic distance was taken into consideration when determining the contrail formation's distribution. However, global averages were once more used to calculate the effect of those contrails on global warming.

Chen and Gettelman [22] investigated modelling the effect of current contrails on the size and structure of cirrus contrail ice crystals. They projected a 7-fold increase in contrail cirrus radiative forcing for 2050 (i.e. $RF_{\mathrm{Contrail}} = 0.087$ $\mathrm{W\,m^{-2}}$) compared to 2006, assuming an average increase in air traffic movements by a factor of 4 till 2050.

II. Radiative Extinction of the Contrail

Before the optical properties of a contrail can be examined, the micro-physical properties have to be calculated along its whole life cycle. In order to focus on the radiative impact of cooling contrails, we refer to external publications, which describe the modelling of the life cycle [16, 17, 23].

The radiation, extinguished by the contrail, comes from all directions in space. The direction $\Omega(\theta, \phi)$ is described by the zenith angle $\theta = [0,\pi]$ and by the azimuthal angle $\phi = [0,2\pi]$. Radiative extinction takes place by scattering (re-directing), absorption (conversion of photons into intrinsic energy) and re-emission (conversion of intrinsic energy into photons with a wavelength according to the higher temperature after absorption of photons) of radiation after interaction with atmospheric molecules, such as contrail ice crystals.

A cooling effect occurs when radiation coming from above is scattered into the upper hemisphere by the contrail (backward scattered). Heating effects occur when either radiation coming from below is scattered into the lower hemisphere, or when radiation is absorbed by the contrail (independent of the direction of incidence). The further the path of a photon through the contrail is (the flatter the angle of incidence), the higher the probability that several scattering events (so-called multi-scattering events) occur to a photon before it is either absorbed or leaves the contrail again.

Radiative extinction due to scattering, absorption, and emission within the contrail is calculated using a Monte Carlo Simulation to take into account multiple scattering events that are likely, especially for large solar zenith angles θ [rad] [16]. This calculation depends on the non-constant geometrical and micro-physical characteristics of the contrail. In the simulation, 10^7 individual photons of a specific wavelength λ and coming from a specific direction (Ω) are tracked on their way through the contrail between location s_1 and s_2 (see Figure 1). For each direction of incoming photons, the number of backward scattered photons (i.e., scattered into the initial hemisphere) is compared with the number of absorbed photons (see Figure 2). Therefore, Beer's law

$$\frac{I_\lambda(s_2)}{I_\lambda(s_1)} = \exp\left[-\int_{s_1}^{s_2} -Q_e\, A_p(s)\, n_p(s)\, \mathrm{d}s\right] = \frac{N_{\mathrm{out}}}{N_{\mathrm{in}}} \quad (1)$$

is utilized, where $I_\lambda(s_1)$ stands for radiation coming from direction $\Omega(\theta, \phi)$ and $I_\lambda(s_2)$ describes the radiation transmitted in the same direction without extinction. The term radiation can be specified by solar intensities $[\mathrm{W\,m^{-2}sr^{-1}}]$ and by terrestrial irradiances $[\mathrm{W\,m^{-2}}]$. The extinction efficiency [-]

$$Q_e(s) = Q_s(s) + Q_a(s) \quad (2)$$

as sum of scattering efficiency $Q_s(s)$ and absorption efficiency $Q_a(s)$ depends on location s, wavelength, particle size and particle shape [16, 24]. $Q_s(s)$ and $Q_a(s)$ determine the probability that a scattering or an absorption event takes place at location s. $A_p(s)$ stands for the projected particle area $[\mathrm{m^2}]$ and the number of ice-particles n_p is hereafter called ice-particle number density $[\mathrm{m^{-3}}]$. Equation 1 is interpreted as number ratio $\frac{N_{\mathrm{out}}}{N_{\mathrm{in}}}$ of extinguished photons of a specific wavelength λ $[\mu\mathrm{m}]$ coming from a direction Ω or from a specific solid angle $\mathrm{d}\omega$

$$\mathrm{d}\omega = \sin\theta\,\mathrm{d}\theta\,\mathrm{d}\phi \tag{3}$$

and is independent of the solar and terrestrial radiation components reaching the contrail [16, 25].

In the simulation, a random number determines the location s, where the next extinguishing event takes place. $Q_s(s)$ and $Q_a(s)$ decide which event takes place and the asymmetry parameter $g_{\mathrm{HG}}(s)$ decides on the scattering angle ϑ of a single scattering event by assuming a distribution of scattering angles following the Henyey-Greenstein phase function $P_{\mathrm{HG}}(\cos\vartheta)$ depending on the asymmetry parameter $g_{\mathrm{HG}}(s)$

$$P_{\mathrm{HG}}(\cos\vartheta) = \frac{1}{4\,\pi}\frac{1-g_{\mathrm{HG}}^2}{(1+g_{\mathrm{HG}}^2-2g_{\mathrm{HG}}\cos\vartheta)^{3/2}} \tag{4}$$

The Henyey-Greenstein phase function satisfies isotropic scattering for $g_{\mathrm{HG}} = 0$, as well as forward and backward scattering for $g_{\mathrm{HG}} = 1$ and $g_{\mathrm{HG}} = -1$, respectively. For solar wavelengths, ice crystals are usually characterized by a strong forward scattering $g_{\mathrm{HG}} \approx 0.8$ [16].

For ice crystals in high altitude cirrus clouds, $Q_s(s)$, $Q_a(s)$ and $g_{\mathrm{HG}}(s)$ are parameterized by Wyser et al. [24] and Yang et al. [26] as functions of wavelength, ice-particle size, shape and density. For a mixture of typical ice crystal shapes with an ice particle radius of $r_p = 10^{-5}$ m, scattering is most likely in the solar spectrum and absorption is typical for terrestrial bands (see Table I with example efficiencies). Hence, for a cooling contrail, the backward scattering of solar photons must compensate the absorption of terrestrial photons.

TABLE I
SOLAR AND TERRESTRIAL SCATTERING Q_s, ABSORPTION Q_a EFFICIENCIES AND ASYMMETRY PARAMETERS $g_{\mathrm{HG}}(s)$ FOR ICE PARTICLE RADIUS OF $r_p = 10^{-5}$ M. VALUES ARE PARAMETERIZED BY [24, 26]

Wavelength [μm]	Q_a	Q_s	g_{HG}
$\lambda = 0.55$	$Q_a = 0.009$	$Q_s = 1.96$	$g_{\mathrm{HG}} = 0.74$
$\lambda = 10.471$	$Q_a \approx 0.24$	$Q_s \approx 0.13$	$g_{\mathrm{HG}} = 0.83$

For each direction of incoming photons, the number ratio $\frac{N_{\mathrm{out}}}{N_{\mathrm{in}}}$ (Equation 1) is used to determine a weighted number ratio $S_i(\lambda, t, \mathrm{d}\omega)$ [m] by

$$S_i(\lambda, t, \mathrm{d}\omega) = \frac{N_{\mathrm{out}}}{N_{\mathrm{in}}} w_{\mathrm{in}} \sin\alpha, \tag{5}$$

where $w_{\mathrm{in}} = 6\hat{\sigma}_h(t)$ denotes the irradiated width of the contrail as a function of the horizontal standard deviation of the contrail width $\hat{\sigma}_h(t)$ [16], see Figure 1. Since the intensity of the radiation depends on the angle between incoming radiation and the irradiated surface, α defines the angle between the length axis of the contrail and the incoming photons

$$\cos\alpha = \sin\theta\,\cos\phi. \tag{6}$$

The simulation is repeated for all spatial directions, described by $\theta = [0, \pi]$ and $\phi = [0, 2\pi]$ with $\mathrm{d}\theta = \mathrm{d}\phi = 2°$. $S_i(\lambda, t, \mathrm{d}\omega)$ is accumulated to number ratios of backward scattered S_b photons with a cooling (blue) and heating (red) effect, forward scattered S_f (black) and absorbed S_{abs} (red) photons (see Figure 2).

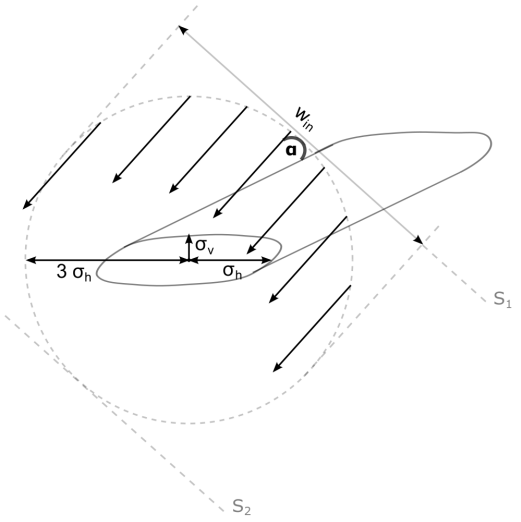

Figure 1. Geometry of the radiative extinction simulation. Photons (black arrows) irradiate the contrail (grey) along the width w_{in} at the angle α to the longitudinal axis of the contrail. The photon's interactions with the ice particles in the contrail are simulated within the observation circle with radius w_{in} between s_1 and s_2.

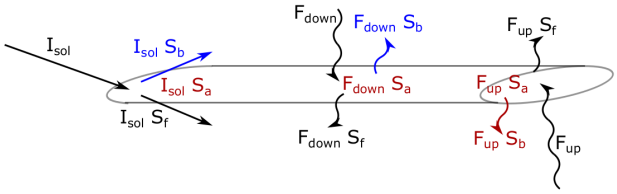

Figure 2. Extinction of radiation (solar: straight arrows, terrestrial: wavy arrows) when photons pass through the contrail. Cooling effects are marked in blue, and warming effects are marked in red.

The weighted number ratios in Figure 3 clearly indicate a strong dependence of the solar cooling (back-scattering) potential on the incoming angles θ and ϕ. Hence, only large solar zenith angles (i.e. horizontal photon transport) hold a cooling potential of contrails.

The longer the travel distance of photons through the contrail (i.e. the larger α and ϕ in Figure 3), the higher the probability that an extinguishing event takes place. With increasing travel distance and with increasing α, the number of out-scattered photons increases, although a dominating forward scattering is expected [24, 26, 27]. This means that compared to vertical photon transport at noon, more photons will be scattered during horizontal photon transport during sunrise and dusk. The power with which the contrail is irradiated, which will be largest at midday and minimum at night, also affects the contrail's radiative extinction.

The terrestrial radiative extinction is dominated by absorption, i.e. heating (Figure 4). The weighted number ratios of absorbed terrestrial photons $S_{\downarrow\uparrow a}$ (heating effect in Figure 4) is in the order of magnitude as the weighted number ratios

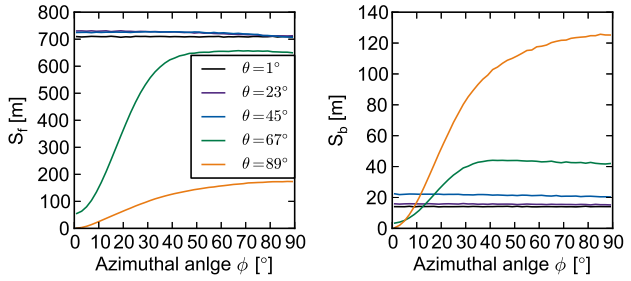

Figure 3. Number ratios of forward S_f (left) and backward S_b (right) scattered photons to the total number of photons ($N_{\text{eval.}} = 10^7$), weighted by the sine of α and by the width w_{in}. The simulation is done for a solar wavelength $\lambda = 0.55$ μm. Only large zenith angles θ enable a cooling contrail effect. The cooling effect is supported for large azimuthal angles ϕ between the contrail axis and incoming photons.

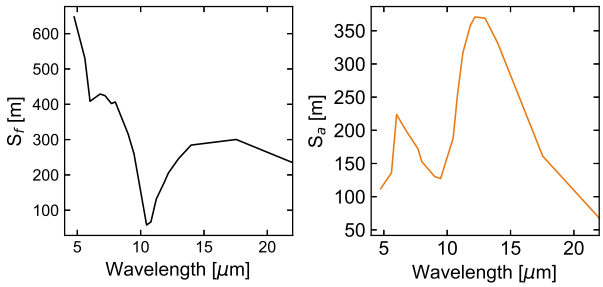

Figure 4. Wavelength-specific simulated number ratios of forward scattered S_f (left) and absorbed S_a (right) photons to the total number of photons ($N_{\text{eval.}} = 10^7$), weighted by the sine of α and by the width w_{in}. The simulation is done for vertical photon transport.

of backward scattered solar photons $S_{\downarrow b}$ (cooling effect in Figure 3).

In order to answer the question under which conditions which effect dominates, the wavelength- and direction-dependent solar intensities or terrestrial irradiances that hit the contrail must first be calculated and then weighted with the extinguished number ratios. For example, for radiation coming from above and getting scattered into the upper hemisphere the extinguished power $P_{\downarrow b}$ [$\mathrm{W\,m^{-1}nm^{-1}}$] is calculated by

$$P_{\downarrow b} = I\, S_{\downarrow b}\, \Omega, \tag{7}$$

where I [$\mathrm{mW\,sr^{-1}m^{-2}nm^{-1}}$] denotes the irradiance coming from the particular solid angle $\mathrm{d}\omega$.

The advantage of the developed method is that the extinguished number ratios (Beer's law, Equation 1) are calculated independently of the unaffected, direction- and wavelength-specific radiation reaching the contrail and can be subsequently combined with any radiation values in Equation 7. For applying, Equation 7 the unaffected solar intensities and terrestrial irradiances are approximated following the results of a radiative transfer model.

III. Atmospheric Radiative Transfer

The contrail extinguishes radiation from three different sources. First, direct solar intensity coming from a single direction $\Omega(\theta, \phi)$ is primarily scattered by the contrail. On the way from the sun to the contrail, this direct solar intensity might be scattered by molecules of the atmosphere in all spatial directions. The result is diffuse solar irradiance from all spatial solid angles $\mathrm{d}\omega$. The solar irradiance and intensity are also absorbed by the Earth's surface and by preferably triatomic molecules of the atmosphere and re-emitted at a longer wavelength. These are terrestrial irradiances. The longer the wavelength of the irradiances, the higher the probability of being absorbed by the atmosphere and Earth's surface.

Approximating the sun and the Earth as a black body, the expected radiative irradiances can be calculated with Planck's function assuming mean temperatures of 5750 K of the sun and 288 K of the Earth's surface. In this case, solar irradiances are expected between $0.2 < \lambda < 1$ μm with a maximum at around $\lambda_{\text{sol}} = 0.55$ μm. Terrestrial irradiances should be considered between $3 < \lambda < 100$ μm with a maximum at around $\lambda_{\text{terr}} = 10.471$ μm [16]. For comprehensibility, the investigations in this study are focused on the two maximum wavelengths λ_{sol} and λ_{terr} representing the solar and terrestrial spectrum. Wavelength, longitude, latitude, altitude, the presence of clouds, time of day, and season all affect solar intensities and terrestrial irradiances before reaching the contrail. The radiative transfer software package libRadtran [28] is utilized to calculate this atmospheric radiative transfer. Details on the calculations of solar intensity and terrestrial irradiances are provided in [17].

Due to the high computational effort for the solution of the radiative transfer equation, it makes sense to approximate the radiation values beforehand and then fall back on tabulated values.

A. Terrestrial Radiative Transfer

The terrestrial wavelength spectrum ($3 \leq \lambda \leq 100$ μm) is modelled with the Two Stream Approximation (TSA) [29], because of a weak angular dependency of terrestrial radiation is anticipated since a contribution of direct irradiance is missing [30]. With TSA all fractions of radiation from a single hemisphere are azimuthally averaged over the half-space (with the solid angle $\mathrm{d}\omega = 2\pi$) and considered as a single irradiance F [$\mathrm{W\,m^{-2}}$] (F_{down} and F_{up}). Figure 5 right, indicates maximum terrestrial irradiances at $\lambda_{\text{terr}} = 10.471$ μm of $F_{\text{up}} = 17.3507$ mW/(m^{2}nm) and $F\text{down} = 0.0199$ mW/(m^{2}nm).

The TSA, however, does not allow a distinction between different surfaces (and temperatures) of the Earth (e.g., snow, ocean, desert,...). The impact of the Earth's surface on terrestrial radiation at flight altitude is under current investigation by the authors.

B. Solar Radiative Transfer

Simplification to lambda max In the solar wavelength spectrum ($0 \leq \lambda \leq 4$ μm) a TSA is not applicable, because of its large dependency on the angle of direct solar intensity.

The radiative transfer solver DISORT (DIScrete Ordinate Radiative Transfer solver) is used for the angular-dependent calculation of direct solar intensities $I_{\mathrm{dir}}(\lambda, t, \mathrm{lon}, \mathrm{lat}, \Omega)$ $[\mathrm{mW\,sr^{-1}m^{-2}nm^{-1}}]$. The direct beam $\Omega(\theta, \phi)$ is described by an infinitesimal solid angle $\Omega(\theta, \phi)$

Diffuse solar irradiances $I_{\mathrm{diff}}(\lambda, t, \mathrm{lon}, \mathrm{lat}, \mathrm{d}\omega)$ $[\mathrm{mW\,sr^{-1}m^{-2}nm^{-1}}]$ depending on longitude, latitude, altitude, time of the day year, and solid angle $\mathrm{d}\omega$ [31] are pre-calculated with DISORT with an angular discretization of $\mathrm{d}\theta = \mathrm{d}\phi = 2°$.

In this study, the angular dependence of I_{diff} with high irradiances coming from $\theta = 90°$, as discussed by Rosenow [16], will be neglected for the investigation of location, time and season of flights with cooling contrails, because, the impact of the direct beam is orders of magnitude greater. For this reason, we approximate hemispherically averaged solar diffuse irradiances $I_{\mathrm{diff}}(\theta, \lambda)$ as a function of solar zenith angle and wavelength.

C. Approximation of Solar Radiative Transfer

From Figures 3 and 5 left, follows a strong dependence of solar radiative extinction on the one hand on the position of the sun and on the other hand on the direction from which the photons irradiate the contrail. Since direct solar radiation is coming only from a single direction, $I_{\mathrm{dir}}(\theta, \lambda)$ is approximated as a function of solar zenith angle and wavelength.

From applying Lambert's cosine law, where the radiant intensity is directly proportional to the cosine of the angle between the direction of the incident photons and the surface normal to the zenith angle θ [32], a dependence of the direct solar intensity from the sinus of zenith angle θ can be expected [30], besides the dependence on wavelength. Therewith, $I_{\mathrm{dir}}(\theta, \lambda)$ is approximated by

$$I_{\mathrm{dir}}(\theta) = a\,\sin(b\,\theta + c), \tag{8}$$

where $a(\lambda = 550\,\mathrm{nm}) = 1763$, $b(\lambda = 550\,\mathrm{nm}) = 0.01718$ and $b(\lambda = 550\,\mathrm{nm}) = 1.62$ are wavelength-specific parameters. The dependence of θ combines the dependence of I_{dir} on latitude, time of day and season and clearly shows the decrease in intensity with increasing zenith angle. It follows that at zenith angles with a high probability of backward scattering (i.e.$\theta \approx 90°$), lower intensities radiate onto the contrail.

Hemispherically averaged diffuse irradiances $I_{\mathrm{diff}}(\theta, \lambda)$ are parameterised depending on the position of the sun and the reflectivity of the Earth's surface. The reflectivity for diffuse upward irradiances is parameterized for 18 surface types defined by the surface library of the International Geosphere Biosphere (IGBP) from the NASA CERES/SARB Surface Properties Project [33]. Figure 6 shows the global distribution of the surface types. Most important for this study are forest classes 1-5, as well as classes 10-13 (see also Table II for class description).

Diffuse downward irradiances above snow (IGBP 15) are twice as high as the irradiances of the other surface types, which hardly differ from each other at a sensor height of

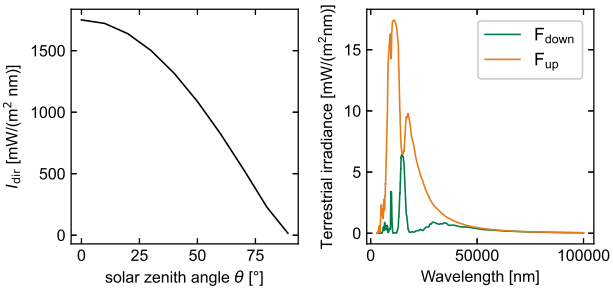

Figure 5. Left: Solar direct intensities as a function of θ modelled with DISORT. Right: terrestrial irradiances at 10 km altitude coming from the upper (F_{down}) and lower (F_{up}) hemisphere modelled with TSA.

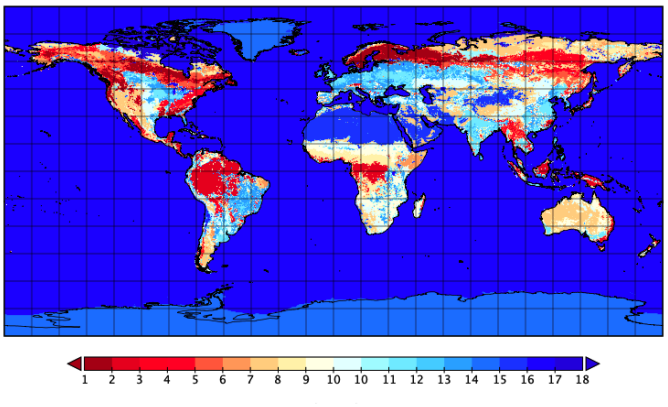

Figure 6. Global distribution of surface types defined by the surface library of the International Geosphere Biosphere Project (IGBP) [33].

TABLE II
IGBP LAND COVER CLASSIFICATION SYSTEM [33].

Nr.	Class name	Nr.	Class name
1	Evergreen needleleaf forests	10	Grasslands
2	Evergreen broadleaf forests	11	Permanent wetlands
3	Deciduous needleleaf forests	12	Croplands
4	Deciduous broadleaf forests	13	Urban and built-up
5	Mixed forests	14	Cropland/natural
6	Closed shrublands	15	Snow and ice
7	Open shrublands	16	Barren
8	Woody savannas	17	Water bodies
9	Savannas	18	Tundra

10 km. Due to the small deviation, the mean value of all the other diffuse downward irradiances is approximated by a single exponential function with two terms of the form

$$I_{\mathrm{diff}}(\theta) = o_1 \exp(p_1\theta) + o_2 \exp(p_2\theta), \tag{9}$$

where $o_1(\lambda = 550\,\mathrm{nm}) = -6.821\,10^{-5}$, $p_1(\lambda = 550\,\mathrm{nm}) = 0.1464$, $o_2(\lambda = 550\,\mathrm{nm}) = 40,63$ and $p_2(\lambda = 550\,\mathrm{nm}) = -1.3\,10^{-3}$ are wavelength-specific parameters. Diffuse upward irradiances of individual surface types deviate more strongly from one another and are parameterised individually for applying Equation 9.

Due to the strongly deviating values and the deviating

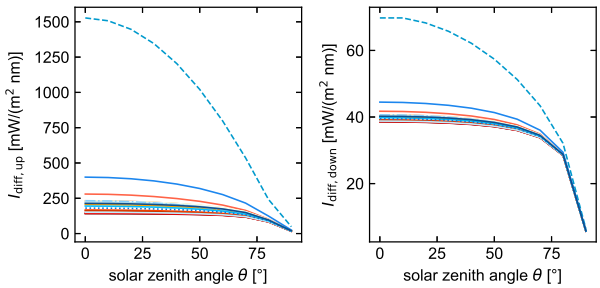

Figure 7. Solar diffuse radiances as function of θ modelled with DISORT in 10 km altitude coming from the lower (I_{up}) (left) and upper (I_{down}) (right) hemisphere. The colour map follows Figure 6 with dashed: snow (IGBP 15), dash-dotted: Urban (IGBP 13), dotted: Water (IGBP 17).

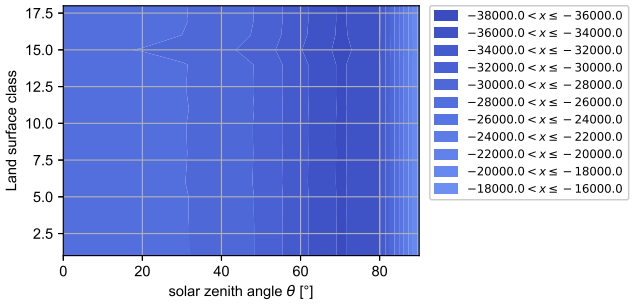

Figure 8. Cooling impact [mW/(m nm)] of extinguished energy of the sun and terrestrial irradiances and sun direct intensities as characteristic of solar zenith attitude and surface type. For all surface types, maximum cooling effects occur for large solar zenith angles between $70° \leq \theta \leq 80°$.

course, diffuse downward irradiances above snow (IGBP 15) are considered separately. Here, a third-degree polynomial function in the form

$$I_{\mathrm{diff,snow}}(\theta) = q_1\theta^3 + q_2\theta^2 + q_3\theta + q_4 \qquad (10)$$

is used with $q_1(\lambda = 550\,\mathrm{nm}) = -3.863\,10^{-5}$, $q_2(\lambda = 550\,\mathrm{nm}) = -2.375\,10^{-3}$, $q_3(\lambda = 550\,\mathrm{nm}) = -0.03289$ and $q_4(\lambda = 550\,\mathrm{nm}) = 70.02$ for downward irradiances above snow and $q_1(\lambda = 550\,\mathrm{nm}) = 8.893\,10^{-4}$, $q_2(\lambda = 550\,\mathrm{nm}) = -0.296$, $q_3(\lambda = 550\,\mathrm{nm}) = 2.372$ and $q_4(\lambda = 550\,\mathrm{nm}) = 1.520$ for upward irradiances above snow.

IV. Conditions of Cooling Contrails

Finally, the parameterized radiative quantities I_{diff}, I_{dir} and F as a function of wavelength and surface type can be combined with the number ratios S_i (Equation 5) of extinguished photons in order to quantify the balance between cooling and heating effects.

From Section III-A follow terrestrial irradiances at $\lambda_{\mathrm{terr}} = 10.471\ \mu m$ of $F_{\mathrm{up}} = 17.3507$ mW/(m^{2}nm) and $F\mathrm{down} = 0.0199$ mW/(m^{2}nm). The combination with S_i from Figure 4 yield net terrestrial heating effect of

$$P_{terr,net} = 32684.6\ \mathrm{mW/(m\,nm)}. \qquad (11)$$

Obviously and supported by Equation 8 follows no dependence of I_{dir} on the land surface class. Hence, the most important cooling contribution is constant for all surface classes but strongly depends on θ.

On the one hand, according to Lambert's cosine law, Equations 8 to 10, as well as Figures 5 and 7 show a decrease in radiation for large θ. On the other hand, the number ratios of upward scattered photons increase with θ. Hence, only small amounts of intensities coming from large θ can contribute to a net cooling effect. Figures 8 to 10 identify a net cooling effect above nearly all surfaces for $70° \leq \theta \leq 80°$.

This effect has to be compensated mainly by the solar direct cooling effect. Although the cooling effects (Figure 8) are inferior to the warming effects (Figure 9, for large solar zenith angles between $70° \leq \theta \leq 80°$ the cooling effect dominates above most of the surfaces.

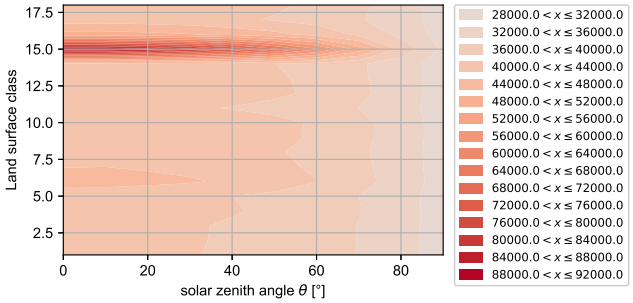

Figure 9. Heating effects [mW/(m nm)] of extinguished solar and terrestrial photons as a function of solar zenith angle and surface type. Red contours indicate maximum warming effects above the snow. Dark blue negative values indicate cooling effects for most surface types at large solar zenith angles between $70° \leq \theta \leq 80°$.

V. Locations and Time of Cooling Contrails

From a scientific point of view, the information on solar zenith angles and surface types with a high potential for cooling contrails might be interesting. However, from an operational point of view, some information on times and locations, characterized by large θ might be more applicable. For this reason, highly frequented air spaces are investigated regarding

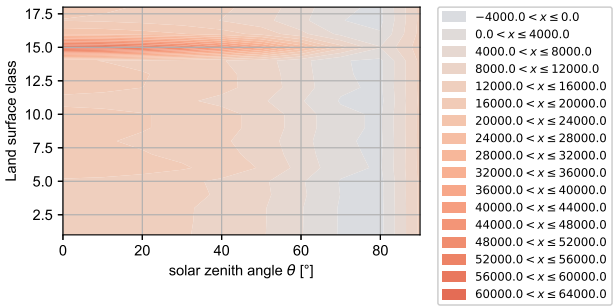

Figure 10. Net effect [mW/(m nm)] of extinguished power of solar and terrestrial irradiances and solar direct intensities as a function of solar zenith angle and surface type. The net warming effect (red contours) is still maximum above the snow. Light blue negative values indicate net cooling effects for most surface types at large solar zenith angles between $70° \leq \theta \leq 80°$.

Earth surface types and θ. First, θ along the North Atlantic Track System (NATS) at latitudes $\approx 55°$ N is investigated in a sun chart (Figure 11). It becomes clear that along the major latitudes in the northern hemisphere, solar zenith angles of $70° \leq \theta \leq 80°$ are common. From September to March the sun does not reach smaller angles θ, and during the summer months, the sun only shines horizontally on the contrail during sunrise and sunset. Note, the solar elevation in Figure 11 is defined as $90° - \theta$.

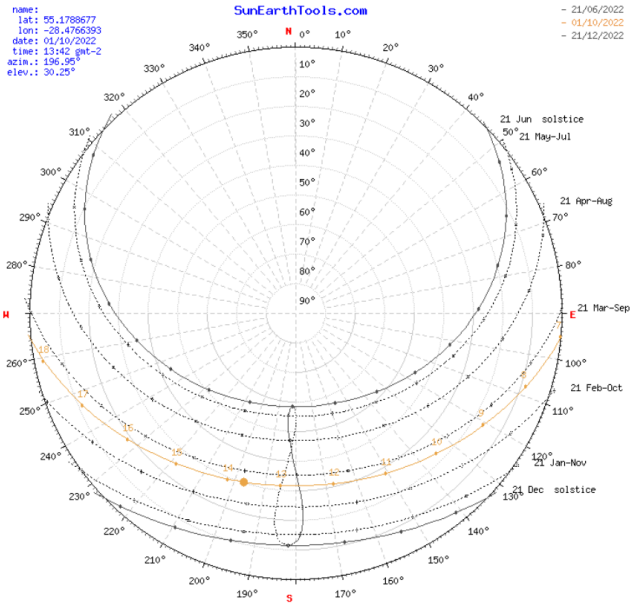

Figure 11. Sun chart diagram for latitude $\varphi = 55°$ N. The axis label of solar elevation is defined as $90° - \theta$. Hence, the solar elevation of 20corresponds to $\theta = 80°$. Along the North Atlantic tracks, the sun is irradiating contrails with $70° \leq \theta \leq 80°$ between September and March the whole day and for the rest year during sunrise and sunset. The diagram is generated with a tool provided by www.sunearthtools.com.

Figure 12 approximates situations in the Northern hemisphere with $70° \leq \theta \leq 80°$, where contrails could cool the atmosphere. Those conditions do not occur near the equator. However, condensation trails are less likely to form at these latitudes due to higher air temperatures. In mid-latitudes, those conditions are fulfilled in the winter time, in the vicinity of the North pole, $70° \leq \theta \leq 80°$ occurs mainly in the summer time. From this follows, that air spaces with highly dense air traffic (i.e. the NATS mid-latitudes in the Northern hemisphere) hold the potential of contrails with a cooling effect. The probability of the cooling effect can be increased when flying during sunrise and sunset.

VI. Conclusion

In this study, conditions of cooling contrails have been investigated. Those conditions can be described at the best by the solar zenith angle θ. We found, the optimal conditions of cooling contrails at $70° \leq \theta \leq 80°$, because horizontal photon transport increases the probability of direct solar radiation scattered into the upper hemisphere. However, the larger the

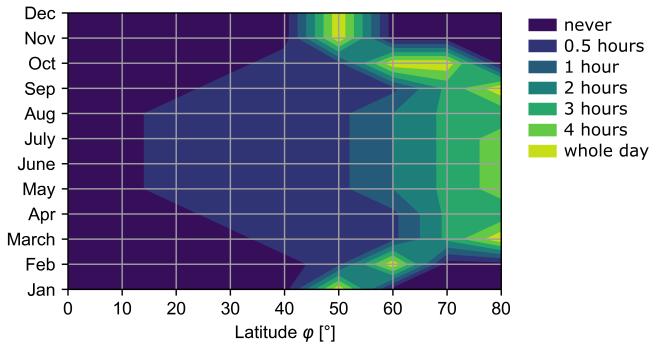

Figure 12. Situations with solar zenith angles between $70° \leq \theta \leq 80°$ described by latitude, month and time of day. For example "whole" stands for all day, and "0.5 hours" means half an hour before and after sunrise and sunset. Conditions with $70° \leq \theta \leq 80°$ have been identified as most beneficial for a dominating cooling effect of contrails

solar zenith angle, the lower the solar intensity irradiated on a horizontal contrail surface. For this reason, $\theta = 90°$ does not yield a maximum cooling effect. The cooling effect of contrails is described by the energy budget at contrail altitude, which is disturbed due to radiative extinction within the contrail. Absorption of photons and backward scattering of photons coming from the lower hemisphere lead to a warming effect which must be compensated by a cooling effect described by backward scattered photons coming from the upper hemisphere. While terrestrial long-wave radiation coming mainly from the lower hemisphere is mainly absorbed, solar direct short-wave radiation coming from the sun is scattered with a higher probability. In our approximation, the terrestrial warming effect is independent of the time and the location of the contrail. A solar warming effect due to scattering and absorption of diffuse solar radiation coming from all directions in space strongly depends on the Earth's surface type beyond the contrail. The solar cooling effect as a result of scattered direct solar radiation significantly depends on latitude, time of the day and year and is summarized in Figure 12.

Finally, we found, that especially mid and high latitudes hold the potential to induce cooling contrails, due to frequently occurring large solar zenith angles. This statement is supported by a higher possibility of contrail formation in those regions. Fortunately, a significant amount of air traffic is taking place in mid and high latitudes. Furthermore, we found that the impact of the land surfaces is not significant, except on snow surfaces, because the contribution of diffuse solar radiation to the energy budget is of minor importance, compared to the impact of the direct beam.

However, in this study, a few simplifications have been carried out, which impact the results and could not be completely quantified. For example, the reduction of the investigation to two single wavelengths has been barely broached by Rosenow [16] but requires additional investigations. Second, the simplification to hemispherically averaged solar diffuse and terrestrial irradiances, although supported by [30] is cur-

rently under investigation by the authors. Finally, an additional natural cloud cover would weaken both the cooling and the warming effect. This was not considered in this study.

However, this paper clearly emphasises that the radiation effect of contrails is strongly direction and sun position dependent and can hardly be quantified in two-dimensional studies with infinitely extended contrails.

References

[1] E. Schmidt, "Die Entstehung von Eisnebel aus den Auspuffgasen von Flugmotoren," *Schriften der Deutschen Akademie der Luftfahrtforschung, Verlag R. Oldenbourg, München/Berlin*, vol. 44, pp. 1–15, 1941.

[2] H. Appleman, "The formation of exhaust condensation trails by jet aircraft," *Bulletin of the American Meteorological Society*, vol. 34, pp. 14–20, 1953.

[3] W. (WMO). Cloud atlas. [Online]. Available: https://cloudatlas.wmo.int/aircraft-condensation-trails.html

[4] R. Meerkötter, U. Schumann, P. Minnis, D. R. Doelling, T. Nakajima, and Y. Tsushima, "Radiative forcing by contrails," *Journal of Geophysical Research*, vol. 17, pp. 1080–1094, 1999.

[5] G. Myhre, D. Shindell, F.-M. Bréon, W. Collins, J. Fuglestvedt, J. Huang, D. Koch, J.-F. Lamarque, D. Lee, B. Mendoza, T. Nakajima, A. Robock, G. Stephens, T. Takemura, and H. Zhang, "Anthropogenic and natural radiative forcing. in: Climate change 2013: The physical science basis. contribution of working group i to the fifth assessment report of the intergovernmental panel on climate change," *Cambridge University Press*, 2013.

[6] D. S. Lee, D. W. Fahey, P. M. Forster, P. J. Newton, R. C. Witt, L. L. Lim, B. Owen, and R. Sausen, "Aviation and global climate change in the 21st century," *Atmospheric Environment*, vol. 43, pp. 3520–3537, 2009.

[7] P. Minnis, U. Schumann, D. R. Doelling, K. M. Gierens, and D. W. Fahey, "Global distribution of contrail radiative forcing," *Geophysical Research Letters*, vol. 26, pp. 1853–1856, 1999.

[8] R. Sausen, I. Isaksen, V. Grewe, D. Hauglustaine, D. S. Lee, G. Myhre, M. Köhler, G. Pitari, U. Schumann, F. Stordal, and C. Zerefos, "Aviation radiative forcing in 2000: An update on ipcc (1999)," *Meteorologische Zeitschrift*, vol. 14, pp. 555–561, 2005.

[9] U. Burkhardt and B. Kärcher, "Global radiative forcing from contrail cirrus," *Nature Climate Change*, vol. 1, pp. 54–58, 2011.

[10] K. Gierens, "Theory of contrail formation for fuel cells," *Aerospace*, vol. 8, no. 6, 2021. [Online]. Available: https://www.mdpi.com/2226-4310/8/6/164

[11] A. Gounou and R. J. Hogan, "A sensitivity study of the effect of horizontal photon transport on the radiative forcing of contrails," *Journal of Atmospheric Sciences*, vol. 64, pp. 1706–1716, 2007.

[12] L. Forster, C. Emde, B. Mayer, and S. Unterstrasser, "Effects of three-dimensional photon transport on the radiative forcing of realistic contrails," *American Meteorological Society*, pp. 2243–2255, 2011.

[13] U. Schumann, "A contrail cirrus prediction tool," in *Intern. Conf. on transport, Atmosphere and Climate, DLR/EUR, Aachen and Maastricht, 22-25 June*, 2009.

[14] U. Schumann, B. Mayer, K. Graf, and H. Mannstein, "A parametric radiative forcing model for contrail cirrus," *American Meteorological Society*, vol. 51, pp. 1391–1405, 2012.

[15] D. Avila and L. Sherry, "Method for calculating net radiative forcing from contrails from airline operations," in *2017 Integrated Communications Navigation and Surveillance (ICNS) Conference*, ser. DOI: 10.1109/ICNSURV.2017.8011927, 2017.

[16] J. Rosenow, "Optical properties of condenstation trails," Ph.D. dissertation, Technische Universität Dresden, 2016.

[17] J. Rosenow and H. Fricke, "Individual condensation trails in aircraft trajectory optimization," *Sustainability*, vol. 11, no. 21, 2019. [Online]. Available: https://www.mdpi.com/2071-1050/11/21/6082

[18] K. Shine, J. Cook, E. J. Highwood, and M. M. Joshi, "An alternative to radiative forcing for estimating the relative importance of climate change mechanisms," *Geophysical Research Letters*, vol. 30, no. 20, 2003.

[19] U. Schumann and K. Graf, "Aviation-induced cirrus and radiation changes at diurnal timescales," *Journal of Geophysical Research*, vol. 118, pp. 1–18, 2013.

[20] K. M. Markowicz and M. L. Witek, "Simulations of contrail optical properties and radiative forcing for various crystal shapes," *Journal of Applied Meteorology and Climatology*, vol. 50, 2011.

[21] L. Bock and U. Burkhardt, "Contrail cirrus radiative forcing for future air traffic," *Atmospheric Chemistry and Physics*, vol. 19, pp. 8163–8174, 2019.

[22] C.-C. Chen and A. Gettelman, "Simulated 2050 aviation radiative forcing from contrails and aerosols," *Atmospheric Chemistry and Physics*, vol. 16, no. 11, pp. 7317–7333, 2016. [Online]. Available: https://www.atmos-chem-phys.net/16/7317/2016/

[23] J. H. J. Rosenow and H. Fricke, "Validation of a contrail life cycle model in central europe," *Aerospace*, p. tba, submitted.

[24] P. Yang, K. N. Liou, K. Wyser, and D. Mitchell, "Parameterization of the scattering and absorption properties of individual ice crystals," *Journal of Geophysical Research*, vol. 105, pp. 4699–4718, 2000.

[25] A. Einstein, "Über einen die erzeugung und verwandlung des lichtes betreffenden heuristischen gesichtspunkt," *Annalen der Physik*, vol. 17, pp. 132–148, 1905.

[26] P. Yang, H. Wei, H.-L. Huang, B. A. Baum, Y. X. Hu, G. W. Kattawar, M. I. Mishchenko, and Q. Fu, "Scattering and absorption property database for nonspherical ice particles in the near-through far-infrared spectral region," *Applied Optics*, vol. 44, pp. 5512–5523, 2005.

[27] A. Macke, P. N. Francis, G. M. McFarquhar, and S. Kinne, "The role of ice particle shapes and size distributions in the single scattering properties of cirrus clouds," *American Meteorological Society*, 2010.

[28] B. Mayer and A. Kylling, "Technical note: The libradtran software package for radiative transfer calculations description and examples of use," *Atmospheric Chemistry and Physics*, vol. 5, pp. 1855–1877, 2005.

[29] A. Kylling, K. Stamnes, and S.-C. Tsay, "A reliable and efficient two-stream algorithm for spherical radiative transfer: Documentation of accuracy in realistic layered media," *Journal of Atmospheric Chemistry*, vol. 21, no. 115-150, 1995.

[30] G. W. Petty, "Area-average solar radiative transfer in three-dimensionally inhomogeneous clouds: The independently scattering cloudlet model," *Journal of the Atmospheric Science*, vol. 59, pp. 2910–2929, 2002.

[31] K. Stamnes, S.-C. Tsay, W. Wiscombe, and K. Jayaweera, "Numerically stable algorithm for discrete-ordinate-method radiative transfer in multiple scattering and emitting layered media," *Applied Optics*, vol. 27, pp. 2502–2509, 1988.

[32] I. H. Lambert, *Photometria sive de mensura et gradibus luminis, colorum et umbrae*. Eberhard Klett, Augsburg, Germany, 1760.

[33] A. Belward and T. Loveland, "The dis 1-km land cover data set," *GLOBAL CHANGE, The IGBP Newsletter*, vol. 27, 1996.